# Design of Progressively Folding Thin-Walled Tubular Components Using Compliant Mechanism Synthesis

Punit Bandi[a], Duane Detwiler[b], James P. Schmiedeler[c], Andrés Tovar[d,*]

[a]*General Motors Company, Detroit, Michigan, 48232*
[b]*Honda R&D Americas, Raymond, Ohio 43067*
[c]*University of Notre Dame, Notre Dame, Indiana, 46556*
[d]*Indiana University-Purdue University Indianapolis, Indianapolis, Indiana, 46202*

**Abstract**

This work introduces a design method for the progressive collapse of thin-walled tubular components under axial and oblique impacts. The proposed design method follows the principles of topometry optimization for compliant mechanism design in which the output port location and direction determine the folding (collapse) mode. In this work, the output ports are located near the impact end with a direction that is perpendicular to the component's longitudinal axis. The topometry optimization is achieved with the use of hybrid cellular automata for thin-wall structures. The result is a complex enforced buckle zone design that acts as a triggering mechanism to (a) initiate a specific collapse mode from the impact end, (b) stabilize the collapse process, and (c) reduce the peak force. The enforced buckle zone in the end portion of the tube also helps to avoid or delay the onset of global bending during an oblique impact with load angles higher than a critical value, which otherwise adversely affects the structure's capacity for load-carrying and energy absorption. The proposed design method has the potential to dramatically improve thin-walled component crashworthiness.

*Keywords:* Thin-walled square tubes, progressive buckling, compliant mechanisms, topometry design, structural optimization, hybrid cellular automata

*Corresponding Author

## 1. Introduction

Thin-walled tubular components are extensively used as structural members in the majority of transportation vehicles because of their low cost, good energy absorption capability, and relatively low density. They have the ability to absorb the kinetic energy of the impacting body in the form of plastic deformation, hence protecting the structure and passengers involved. These structures can be used in various loading conditions such as axial crushing, bending, oblique impact, and transverse loading. Tubular structures show significant energy absorption for long strokes in an axial crushing mode and, therefore, present an attractive option in crashworthiness designs.

A great deal of research has been done to study the axial crushing of thin-walled tubes since the pioneering work of Pugsley [1] and Alexander [2] during the 1960s. In the 1980s, work on both the static and dynamic responses of tubes focused more on theoretical and experimental studies [3, 4]. The concept of a superfolding element was introduced by Wierzbicki and Abramowicz [5] to better understand the crushing mechanics of thin-walled structures. With the advancement in computing power and the numerical implementation of finite element methods in the last two decades, considerable work has been done to create equivalent numerical models for tube crushing and their validation with experimental tests [6, 7, 8, 9]. With the help of advanced nonlinear software like LS-DYNA and ABAQUS, results from numerical models of axial and oblique loadings of thin-walled structures sufficiently match experimental results.

Various experimental and numerical studies revealed three dominant modes of deformation during the axial crushing of thin-walled structures: progressive buckling, global or Euler-type buckling, and dynamic plastic buckling [10]. Of these three, the progressive buckling mode is desired for crashworthy designs because of its efficient energy absorption and better force-displacement behavior. In progressive buckling, crushing starting at one end (often the end close to the impact) and progressing systematically toward the other end of the structure is preferred since it utilizes the maximum possible material for plastic deformation without jamming. Also, the progressive buckling from the front end to the back end helps to protect important components close to or behind these energy absorbing structures. For example, the damage for low intensity ($\sim$ 7-10 mph) frontal impacts in automobiles can be restricted to the bumper-beam and crash-box (hence saving the front frame-rail behind them) if the crash-box collapses progressively without jam-

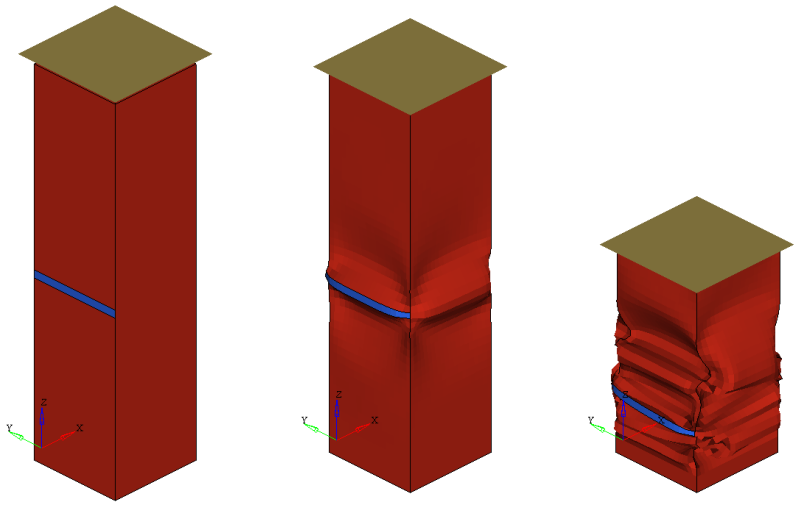


Figure 1: Progressive collapse of a thin-walled tubular component with a geometric imperfection (blue stripe) under axial crushing load by a rigid plate.

ming. Thin-walled square tubes, however, do not buckle progressively from the front end to the back end in all cases. The buckling behavior is dependent on many factors such as loading conditions, geometry, imperfections, and asymmetries in the structure. For example, Fig. 1 shows the deformation under axial compression of a tube of uniform thickness (1 mm) except for a small imperfection in the form of a patch (blue stripe) of thickness 0.8 mm. It can be seen that buckling starts at the location of the imperfection and then progresses in both directions. Interestingly, for this model, even though the imperfection is located in one single face, the initial progressive buckling mode is extensional; in other words, the four collapse elements (one per face) "extend" outwards (see Sec. 2).

Collapse initiators, also known as triggers, stress concentrators, or imperfections, can be used to initiate a specific axial collapse mode, stabilize the collapse process, and reduce the peak force during the axial crush [11, 12, 13]. Researchers have proposed ways of introducing buckle initiators or surface patterns to enhance energy absorption and buckling behavior by introducing various crush zones in the structure in the form of chamfering [14], dents [15], multi-corners [16], multi-cells [17, 18], diamond notches and holes [19], triggering dents, circumferential grooves and stiffeners [20]. The use of col-

lapse initiators has been demonstrated to reduce sensitivity to geometric and material imperfections, reduce peak crushing force, and increase energy absorption density; however, its effectiveness largely depends on the direction of the load and the general shape of the component. An overview of techniques using geometric and material modifications to improve the buckling behavior and energy absorption characteristics of thin-walled tubes under axial crushing can be found in a review article by Yuen and Nurick [21].

During an actual crash event, the tubular structure will seldom be subjected to pure axial loads. Thin-walled structures are subjected to both axial forces and bending moments in an oblique crash. During the study of thin-walled tubes under oblique impacts, Han and Park [22] and Reyes et al. [23] observed a phenomenon of the onset of global bending or Euler-type buckling if the load angle was higher than a critical value. This onset of global bending severely reduces the energy absorption capability of tubular component.

In the methodology presented here, thickness-based (topometry) design [24] is extended to thin-walled square tubes under axial compression using compliant mechanism synthesis [25]. The ability of compliant mechanisms to transfer motion and forces from an input load location to the desired points in the structure is utilized to achieve the desired buckle zones in the axial member. By suitably defining the output port locations and desired displacement directions, progressive buckling can be initiated at the desired locations. Moreover, using this method, thin-walled structures can be designed to show progressive buckling even in cases of oblique impact at angles higher than the critical value at which bending collapse dominates the axial collapse and leads to poor energy absorption. To perform thickness-based topometry design of mechanisms, the structural synthesis method for compliant mechanism of Bandi et al. [25] is modified by using thickness as the design variable. In the following sections, a detailed description of the proposed method and two illustrative examples are presented.

## 2. Progressive Buckling in Square Tubes

During pure axial crushing of a thin-walled tubular component, the maximum peak force ($F_{max}$) appears when the structure starts buckling for the first time, and after that, the force oscillates between local peaks and minima as shown in Fig. 2. Each pair of peaks is associated with the development of a wrinkle or buckle. Usually, these wrinkles or buckles develop sequentially from one end of a tube so that the phenomenon is known as progressive

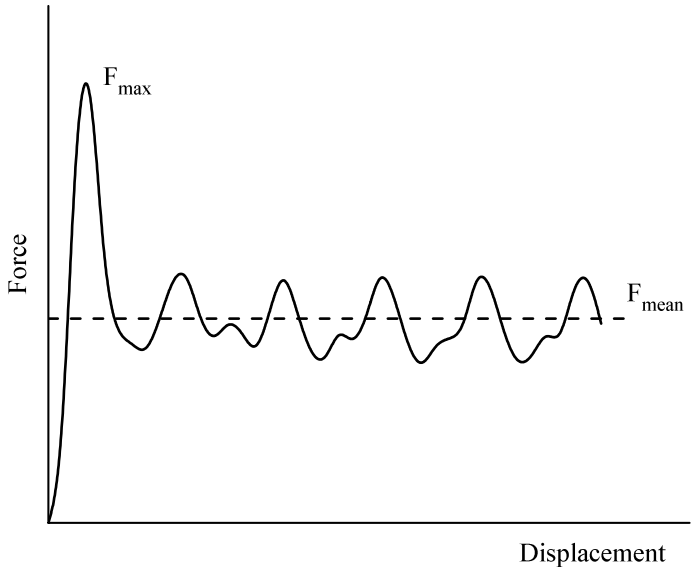


Figure 2: Typical force-displacement curve for an axially crushed thin-walled square tube. This particular curve is the response of a thin-walled square tube of width 100 mm and thickness 3 mm impacted at 5 m/s.

buckling. Designers often ignore the oscillations in the force-displacement behavior and use a mean value ($F_{mean}$) as an indicator of the energy absorption capability.

Two basic forms of collapse elements have been identified by Wierzbicki and Abramowicz [5]: Type I and Type II (Fig. 3). These basic elements have been used to study the progressive buckling of square tubes with mean width $w$ and mean wall thickness $t$. Based on the geometric compatibility requirements at the vertical interfaces of the basic elements, there are four different collapse modes: symmetric mode, extensional mode, asymmetric mode A, and asymmetric mode B. The symmetric crushing mode consists of four Type I collapse elements in each layer of folds. Therefore, in each fold subjected to symmetric crushing, two of the parallel faces of the tube move inward while the other two parallel faces move outward. This mode of crushing is dominant in thin square tubes with $w/t > 40.8$. The extensional collapse mode consists of four Type II collapse elements in each layer of fold, so all faces move outwards. This mode of crushing is dominant in thin square tubes with $w/t < 7.5$. The asymmetric mode A consists of two adjacent layers of folds having six Type I and two Type II basic collapse elements.

The asymmetric mode B consists of two adjacent layers of folds having seven Type I and one Type II basic collapse elements. Asymmetric modes A and B are predicted to take place within the range $7.5 < w/t < 40.8$. In the present work, tubes are designed to promote a symmetric mode of collapse by defining output ports on the two parallel faces pointing inward.

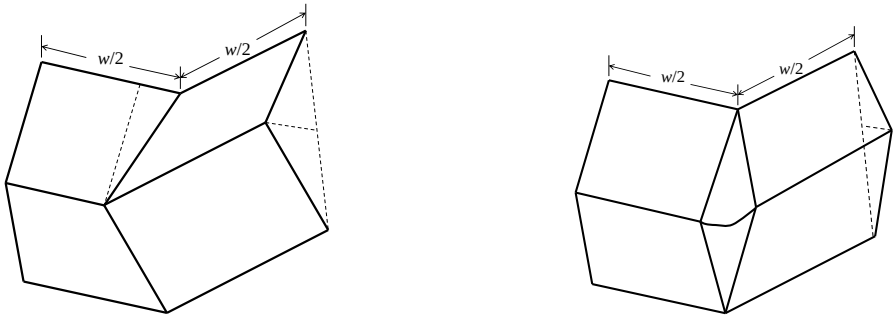


(a) (b)

Figure 3: Basic collapse element shapes for a quarter of a square cross section of a tube with width $w$: (a) Type I and (b) Type II.

## 3. Compliant Mechanism Design in Topology Optimization

The objective of a compliant mechanism is to efficiently transfer forces and motion from an input actuation location (referred to as input port) to desired output locations (referred to as output ports) in a structure. In the design of a compliant mechanism, there are no restrictions on the locations of the ports; however, input and output ports typically correspond to separate points (or set of points) in the structure's boundary. The related optimization problem is to find the optimal material distribution that maximizes the displacement at the output ports subjected to a mass equality constraint [26, 27]. The displacement at an output port $d_{out}$ can be represented in an energy-like functional quantity known as mutual potential energy (MPE) [28, 29]. This is

$$d_{out} \equiv MPE = \mathbf{F}_d^{\mathrm{T}} \mathbf{D}_1 = \int_{\Omega} \boldsymbol{\sigma}_d^{\mathrm{T}} \boldsymbol{\epsilon} \, \mathrm{d}\Omega, \tag{1}$$

where $\mathbf{F}_d$ can be thought of as the vector of "dummy" or fictitious forces of unit magnitude acting at the output port in the direction of the desired output displacement and $\mathbf{D}_1$ is the vector of nodal displacements resulting from

the input load. Notably, the dummy loads are applied at the output ports while the input displacements are obtained at the input ports. Similarly, $\boldsymbol{\sigma}_d$ is the stress field due to the dummy load, and $\boldsymbol{\epsilon}$ is the strain field due to the input load. Dummy loads are not physical. In compliant mechanism design, they are used as an alternative way to express output port displacement in terms of an energy functional quantity such as MPE. This enables separation of local energy contributions from individual elements. Hence, the optimization problem of maximizing the output port displacement subject to a mass equality constraint can be written as

$$\begin{array}{rl} \text{find} & \mathbf{x} \in \mathbb{R}^n \\ \text{minimize} & -MPE(\mathbf{x}) \\ \text{subject to} & \frac{1}{n}\sum_{i=1}^{n} x_i = M_f^* \\ & 0 < x_{\min} \leq x_i \leq 1 \quad \text{for} \quad i = 1, \ldots, n, \end{array} \tag{2}$$

where $x_i$ is the design variable that characterizes the material property of the element of the structure at the discrete location $i$. In the context of topology optimization, $x_i$ is referred to as an "artificial" or relative material density [27]. In particular, $x_i = (E_i/E_0)^{1/p}$, where $E_0$ is the Young's modulus of the material, $E_i$ is its interpolated value, and $p$ is a penalization factor usually selected to be $p = 3$. $M_f^*$ represents the target mass fraction corresponding to the sum of the element masses with unit volume.

To calculate the MPE, a dummy load method is used in which two load cases are considered [29]. In the first load case, an input force at the input ports is applied. In the second load case, a unit dummy load is applied at the output port in the direction of the desired displacement. The MPE is defined based on these two load cases, and Eq. (1) is then used to determine the work (response) of the input loads at the output port locations. The optimization algorithm incorporated in this work is the hybrid cellular automata (HCA) algorithm originally proposed by Tovar et al. [30]. The HCA algorithm is an approach inspired by the bone functional adaptation process in which local evolutionary rules, obtained from classical control theory, iteratively establish the value of the design variables (or cellular automata) that minimize the local error between a so-called field variable and a corresponding set point. The expression for the field variable and the set point are derived from the problem's Karush-Kuhn-Tucker (KKT) optimality conditions [31]. The HCA algorithm has been extended to design non-linear compliant mechanisms by Bandi et al. [25, 32].

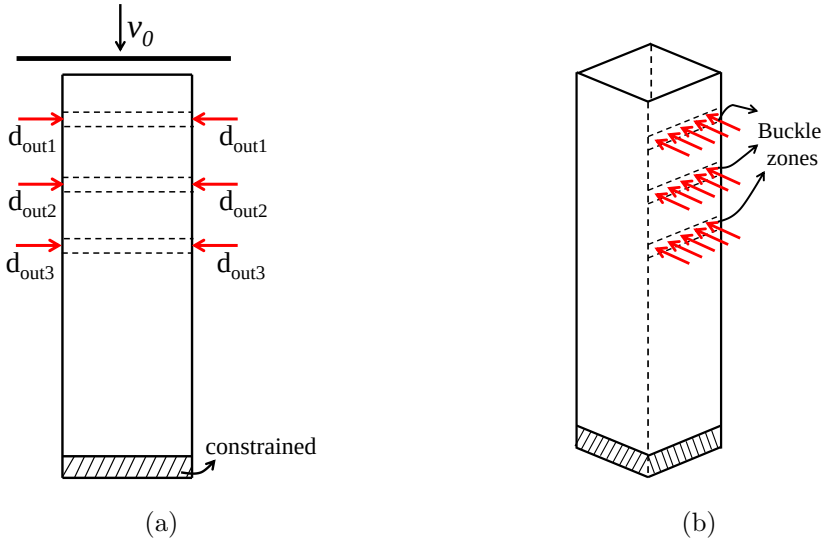


Figure 4: Three sets of output ports, pointing inward, defined on the two parallel faces to trigger buckling. (a) Front view showing the impacting wall at a velocity $v_0$. (b) Isometric view of the output ports (enforced buckle zones) in one of the parallel faces.

## 4. Methodology

Using the proposed compliant mechanism method, thin-walled square tubes can be designed to undergo progressive buckling starting from the front end during axial crushing regardless of geometric and material imperfections, asymmetries in the tube geometry, and loading conditions. The underlying principle is to design the tube using a compliant mechanism approach to trigger the symmetric mode of collapse near the impact end. Figure 4 shows three sets of inward-pointing output ports on two parallel faces of the square tube. The deformation is initiated at these ports in the pointing direction and, hence, forms a fold or wrinkle with four Type I elements per layer (three layers in this case). The location of the output ports along the length of the tube is referred to as the "enforced buckle zone" in subsequent discussions.

The compliant mechanism design approach described in Section 3 is modified to perform thickness-based (topometry) design changes. For plane stress elements, the variation in relative density and thickness has the same effect on the element stiffness tensor [27]. Since plane stress shell elements are used to model thin-walled structures, relative density $\mathbf{x}$ can be replaced by

the element thickness $\mathbf{t}$ in the compliant mechanism problem formulation as

$$\begin{array}{rl} \text{find} & \mathbf{t} \in \mathbb{R}^n \\ \text{minimize} & -MPE(\mathbf{t}), \\ \text{subject to} & \frac{1}{n}\sum_{i=1}^{n} t_i = T^*, \\ & 0 < t_{\min} \leq t_i \leq t_{\max} \quad \text{for} \quad i = 1, \ldots, n. \end{array} \tag{3}$$

The original mass equality constraint is reformulated as an equality constraint on the average thickness value. The dummy load method is used to evaluate mutual potential energy (MPE) with the help of two load cases (see Sec. 3). In the first load case, the dynamic axial crushing caused by the rigid plate is approximated by static axial loads, while in the second load case, a dummy load $F_d$ is applied at the output ports in the direction of the desired displacement. Here again the HCA algorithm is used to solve the optimization problem. Once the tube is designed to transfer motion and forces from the input loading points to the prescribed output points efficiently with the approximated static loading, it will behave in a similar fashion with the application of actual dynamic loading. The enforced buckle zones act as triggering mechanisms and help to reduce the peak force by facilitating the formation of folds with less resistance. In addition, these enforced buckle zones delay or completely eliminate the onset of global bending (Euler-type buckling) during oblique impacts with load angles higher than the critical value.

## 5. Examples

In the following two examples, the explicit nonlinear finite element code LS-DYNA is used to perform dynamic simulations of axial crushing of square tubes. A linear elastic, piecewise linear plastic material (*MAT24) is used for modeling steel tubes with properties shown in Table 1.

Generally, thin-walled structures under axial compression are modeled with plane stress shell elements. In several investigations [33, 7], reasonable agreement has been found between shell-based finite element simulations and experimental results. This work models tubes using a very efficient plane stress shell element formulation from LS-DYNA (ELFORM=16) that is not subject to hourglassing (spurious strain energy modes) due to four in-plane integration points. Five integration points are used throughout the thickness in order to capture the local element bending accurately. This element is a fully integrated shell with assumed strain interpolants used to

Table 1: MATERIAL PROPERTIES OF STEEL USED FOR MODELING SQUARE TUBES

| Property | Value |
|---|---|
| Density | 7800 kg/m$^3$ |
| Elastic Modulus | 207 GPa |
| Poisson's Ratio | 0.29 |
| Yield Stress | 253 MPa |

| Effective plastic strain | Effective stress (MPa) |
|---|---|
| 0.000 | 253 |
| 0.048 | 367 |
| 0.108 | 420 |
| 0.148 | 442 |
| 0.208 | 468 |
| 0.407 | 524 |
| 0.607 | 561 |
| 0.987 | 608 |

alleviate locking and enhance in-plane bending behavior [34]. Fracture is not considered in this analysis.

The examples in this section consider thin-walled structures of high width-to-thickness ratio, $w/t > 40.8$, which are commonly found in automotive applications. The design process is performed on structures that are free of geometric and material imperfections and are subjected to axial loading. The reason is that the exact features of the imperfections and the direction of the load are unknown. Hence, the idea of the present work is to obtain a design that behaves in a desired predictable manner even in the presence of unexpected imperfections and/or oblique impact.

### *5.1. Progressive Buckling in the Presence of an Imperfection*

This example considers the axial crushing with a rigid flat plate of a thin-walled square tube constrained at one end. The tube is 200 mm long, and the square cross section is 50 mm wide. The tube has a uniform thickness of 1 mm, except an imperfection is added in the form of a small patch (4 mm long) of thickness 0.8 mm in the middle of one face. The schematic of the tube and the location of the imperfection are shown in Fig. 5 (all dimensions are in mm.). The rigid plate, which has a mass of 147 kg, is given an initial velocity $v_0$ (3, 5 and 10 m/s). The contact between the rigid plate and the tube is modeled using a constraint algorithm (*CONTACT_AUTOMATIC_NODES_TO_SURFACE) with a friction coefficient of 0.3 to allow sliding movement. To account for the contact between the lobes (folds) during deformation, a single surface contact algorithm with a coeffi-

cient of friction 0.1 is used [35].

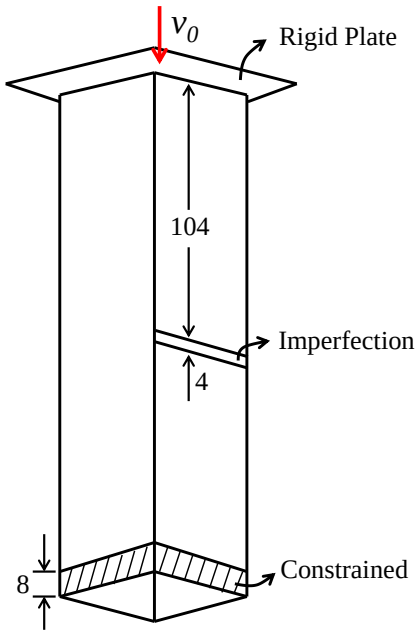


Figure 5: Schematic of a thin-walled square tube with an imperfection impacted axially by a rigid plate.

A mesh convergence study is performed with various mesh refinements and two values of initial velocity $v_0$ for the impacting rigid plate. The force-displacement behavior, amount of energy absorption, and lobe (fold) formation pattern are used to evaluate the mesh size sufficiency. Depending on the mesh size, a single-precision dynamic crush simulation takes between 2 and 10 hours on LS-DYNA V971 R6.1.2 (R6.85274) running in parallel on eight 2.4 GHz dual Intel E5645 processors with 24 GB of RAM. The results corresponding to the three representative mesh sizes are shown in Figs. 6 and 7. The mesh resolutions referred to in the figures correspond to the total number of elements in the square perimeter by the number of elements along the length of the tube. For all three mesh resolutions and two cases of initial velocities, the first fold forms at the imperfection. The next fold for the 80×50 mesh model forms above the first fold, whereas it forms below the first fold for the other two finer mesh models. This difference in deformation pattern for the 80×50 mesh model is also reflected in the force-displacement

behavior and the amount of energy absorption. Qualitatively, the deformation pattern and force-displacement behavior for the 100×100 and 200×200 mesh models are very similar in terms of locations of lobe formation and corresponding peaks in the force-displacement curves.

The peak force and the total energy absorption values are used to quantitatively compare the three models. The peak force with initial velocity of 3 m/s for the three models starting with the coarsest mesh are 47777 N, 44481 N, and 43526 N, respectively. Similarly, the peak forces for the three models with initial velocity of 5 m/s are 51814 N, 50389 N, and 49367 N, respectively. Figure 7 shows the variation in total energy absorption with mesh refinement for initial velocities of 3 m/s and 5 m/s. Clearly, the difference in values corresponding to the models with 100×100 and 200×200 mesh resolutions is comparatively smaller than the difference between the models with 80×50 and 100×100 mesh resolutions. In order to be more confident about the quantitative convergence, one more model with even higher mesh resolution (such as 300×300) could be used, but the simulation time increases dramatically for higher resolutions as the time-step size in an explicit scheme is dependent on the smallest element size in the model. Hence, based on the reasonable similarities between the models with 100×100 and 200×200 mesh resolution and computational practicality, a mesh resolution of 100×100 (element size of 2 mm × 2 mm) is used for the subsequent design process. During the design process, the actual crushing load is replaced by the input and output dummy loads and the simulation time is reduced from a few hours to about 5 minutes.

Two cases with different impact velocity are considered: 3 m/s and 5 m/s. In each case, the buckling starts at the imperfection and can progress in any direction. The deformation patterns for two representative cases are shown in Figs. 8 and 9. In both cases, the simulation is carried out for 0.03 seconds. For the impact with an initial velocity of 3 m/s, the subsequent folds form below the first fold, whereas the subsequent folds form above the first fold when the impact velocity is 5 m/s. The buckling behavior is often affected by the presence of imperfections (e.g., geometric, material, manufacturing), and depending on their location, the buckling can be triggered in the middle or lower end of the tubular component. Moreover, the direction of the progressive buckling (subsequent fold formation) depends on many factors, and it is difficult to predict.

The resulting thickness distribution, which follows the compliant mechanism approach, promotes progressive fold formations starting from the output

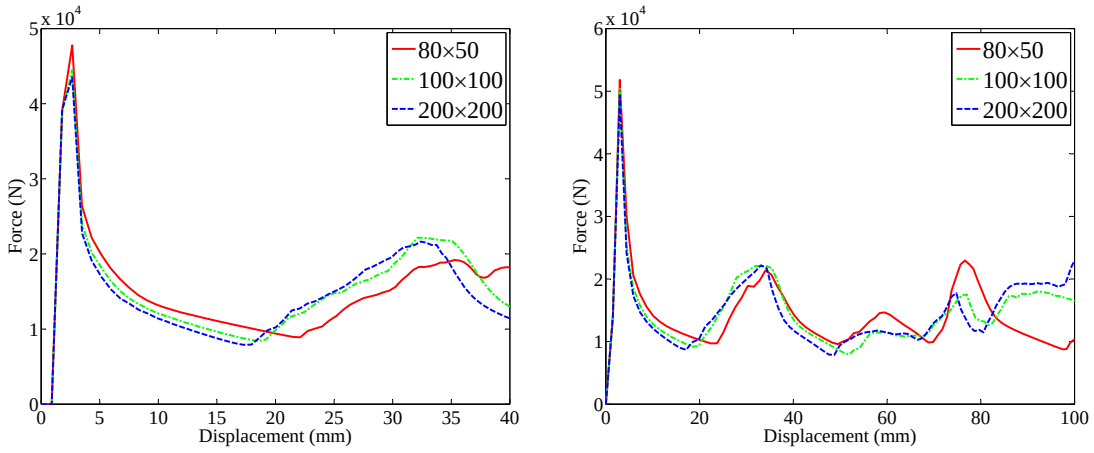


Figure 6: Force-displacement behavior comparison of the square tube under axial impact modeled with three different mesh resolutions for impact velocities (a) $v_0 = 3$ m/s and (b) $v_0 = 5$ m/s.

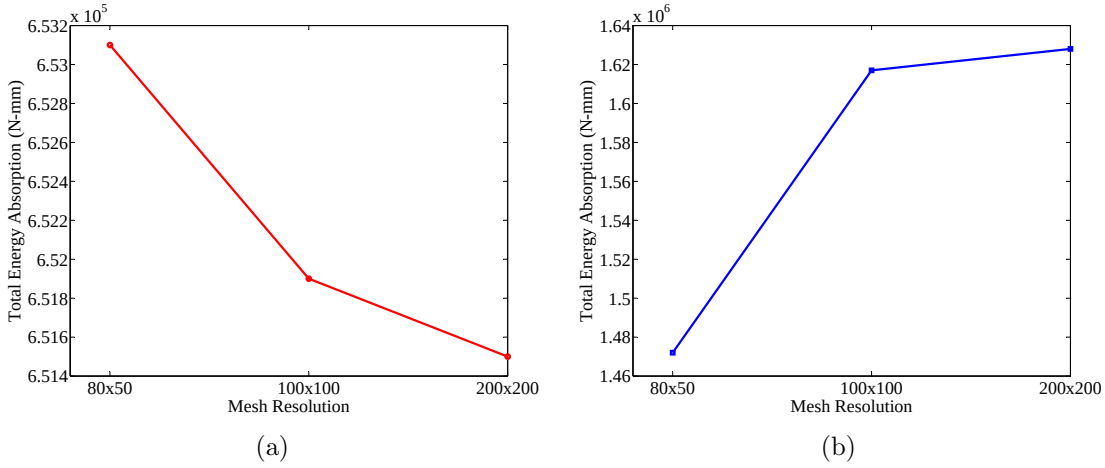


Figure 7: Variation in total energy absorption of the uniformly thick tube under axial impact modeled with three different mesh resolutions for impact velocities (a) $v_0 = 3$ m/s and (b) $v_0 = 5$ m/s.

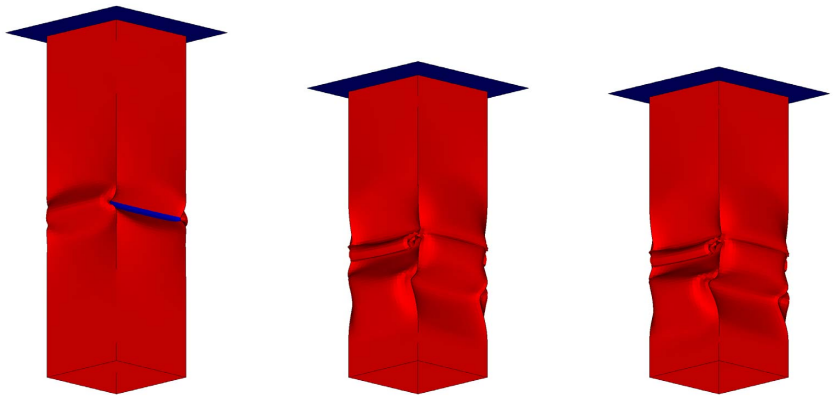

(a) (b) (c)

Figure 8: Deformation of the uniformly thick tube with an imperfection at various times when impacted axially by a rigid plate with an initial velocity of 3 m/s at simulation times (a) 0.003 s, (b) 0.021 s, and (c) 0.030 s.

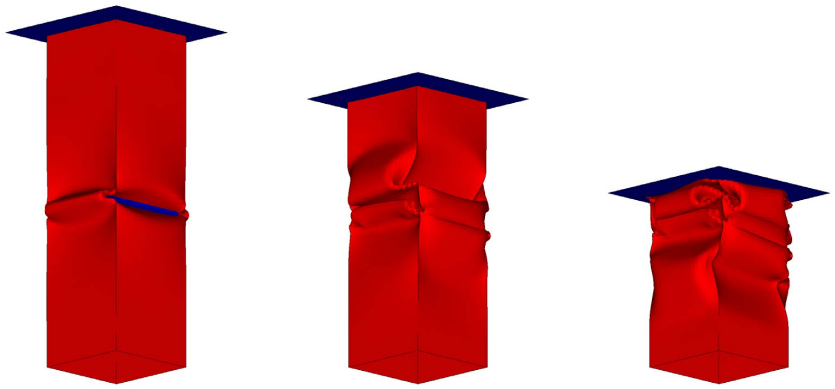

(a) (b) (c)

Figure 9: Deformation of the uniformly thick tube with an imperfection at various times when impacted axially by a rigid plate with an initial velocity of 5 m/s at simulation times (a) 0.003 s, (b) 0.021 s, and (c) 0.030 s.

port location in the impact end. In the present example, one set of output ports close to the loading end is defined as shown in Fig. 10(a). The output ports defined at a distance of 24 mm from the free end of the tube on the two parallel faces A and A' (not visible in the figure) point inward. The choice of location for the output ports is user- and problem-dependent, but a reasonable location would be half the wavelength of deformation (during the axial crushing of a uniformly thick tube) away from the free end. The wavelength of deformation is the distance between two successive folds [15]. It indicates the average length of the tube consumed in one fold during progressive buckling. As mentioned earlier, the dummy load method is used to synthesize a structure having compliant-mechanism-like behavior such that the faces A and A' move inward at the location of the output ports to facilitate a (symmetric mode) fold. The thickness variable is allowed to vary between an upper bound ($t_{\max}$) of 1.2 mm and a lower bound ($t_{\min}$) of 0.8 mm. The average thickness target ($T^*$) is set to 1 mm so that the final mass of the designed tube is the same as the mass of the original uniformly thick tube.

Figure 10(b) shows the thickness distribution of the designed tube. The "hour glass" shaped patch of maximum allowable thickness $t_{\max}$ on face A (and A') creates a stiffness distribution that forces the center of it to move inward. The corresponding thickness distribution on face B (and B') ensures that it moves outward at the same location as the output ports on face A. The deformation behavior of this designed tube for the two initial velocities of impact (3 m/s and 5 m/s) is shown in Figs. 11 and 12. It can be seen that the buckling starts at the desired location in the desired mode (symmetric) and progresses systematically to the other end for both cases even in the presence of the imperfection. A similar deformation behavior is observed for several variations in the impact velocity and the mass of the rigid plate.

Figure 13 compares the force-displacement behavior of the designed tube with that of the original uniformly thick tube for initial velocities of 3 m/s and 5 m/s. For the impact with an initial velocity of 3 m/s, the designed tube has a significant reduction in the peak force at the cost of increased displacement. This can alternatively be stated as the designed tube being more flexible compared to the uniformly thick tube. This is due to the enforced buckle zone in the designed tube that helps initiate (trigger) the buckling. The drop in the peak force for the designed tube is desired since it helps to reduce injury, whereas an increase in displacement, although not desired, can be afforded because thin-walled structures are typically employed

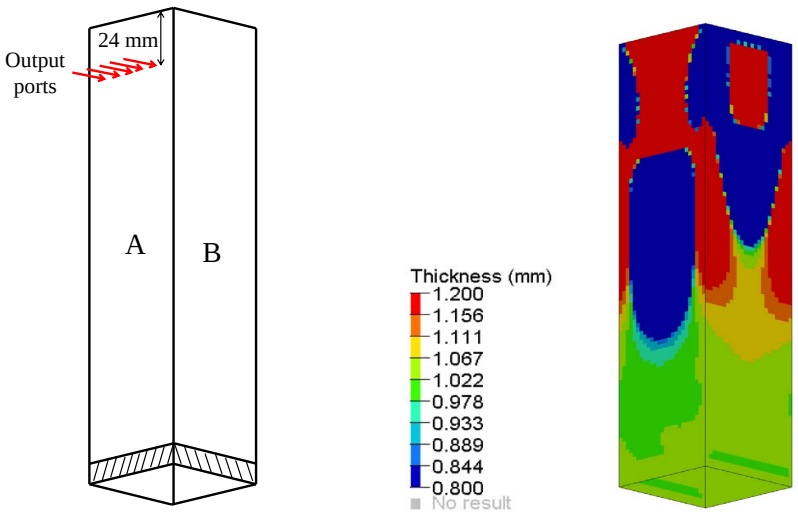


Figure 10: Optimal design of a thin-walled structure with a single set of output ports: (a) output port definition, and (b) thickness distribution for the designed tube.

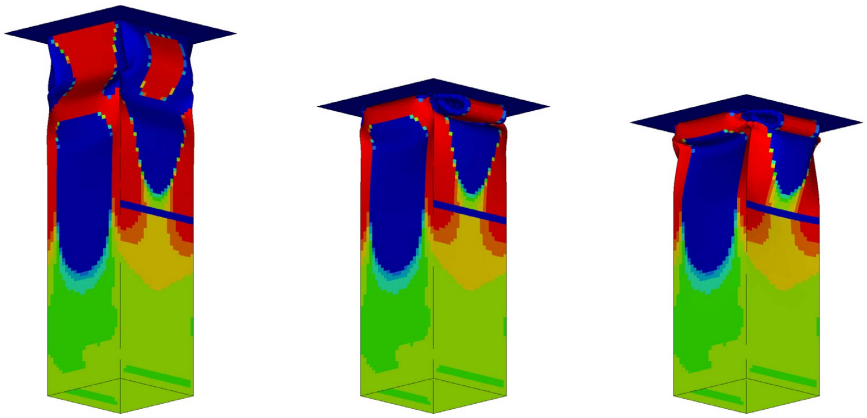


Figure 11: Deformation of the designed tube with an imperfection at various times when impacted axially by a rigid plate with an initial velocity of 3 m/s at simulation times (a) 0.003 s, (b) 0.021 s, and (c) 0.030 s.

to withstand long strokes. A similar effect (drop in peak force and increase in displacement) is also seen when the impact velocity is 5 m/s, although the drop in the peak force is not very large because the intensity of the impact is

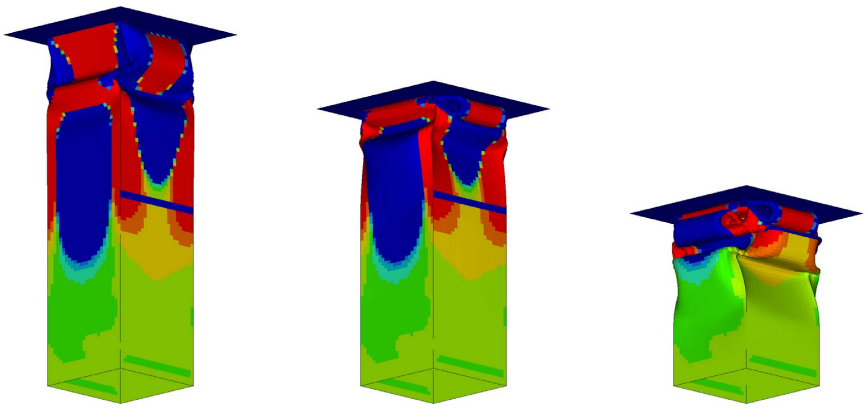

(a) (b) (c)

Figure 12: Deformation of the designed tube with an imperfection at various times when impacted axially by a rigid plate with an initial velocity of 5 m/s at simulation times (a) 0.003 s, (b) 0.021 s, and (c) 0.030 s.

high in that case. Table 2 shows the quantitative comparison of the designed tube and the original uniformly thick tube. All values are recorded for the simulation time of 0.03 seconds. While increased flexibility reduces the peak force, it also reduces the amount of energy absorption as the designed tube shows less resistance to deformation. Nevertheless, the longer stroke due to the increased flexibility of the designed tube helps to recover some additional energy absorption.

Table 2: QUANTITATIVE COMPARISON OF THE BEHAVIOR OF THE DESIGNED TUBE AND THE ORIGINAL UNIFORMLY THICK TUBE UNDER AXIAL IMPACT

| | Peak Force (N) | Displacement (mm) | Total Energy Absorbed (N-mm) |
|---|---|---|---|
| Uniform ($v_0 = 3$ m/s) | 44481 | 42.70 | 651867 |
| Designed ($v_0 = 3$ m/s) | 37871 | 56.16 | 634788 |
| Uniform ($v_0 = 5$ m/s) | 50389 | 104.8 | 1617130 |
| Designed ($v_0 = 5$ m/s) | 45087 | 110.4 | 1414770 |

The proposed method has been demonstrated to result in a design with the desired buckling behavior in the present example. The designed tube under axial impact shows progressive buckling starting from the loading end, and the enforced buckle zone helps to reduce the peak force. In longer tubes,

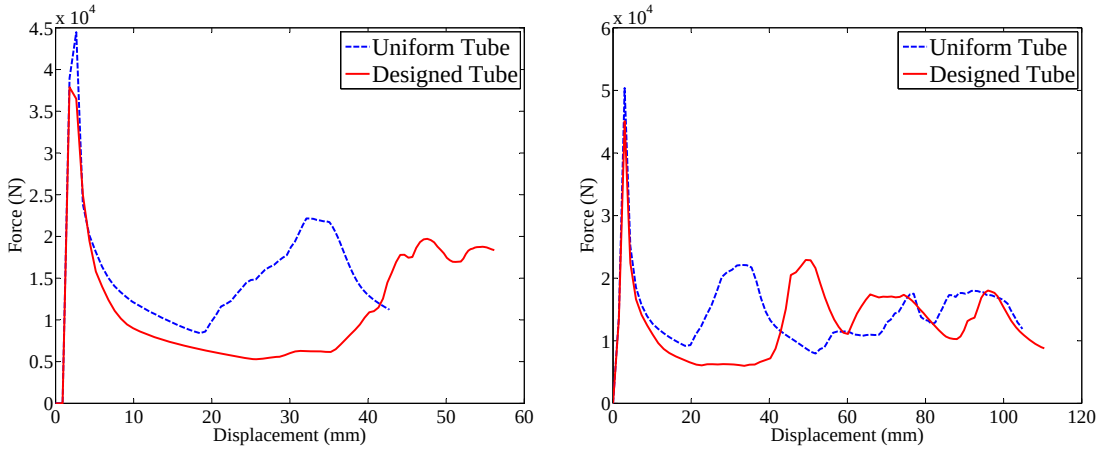


(a) (b)

Figure 13: Comparison of the force-displacement behavior of the designed tube and the original uniformly thick tube during axial impact at impact velocities (a) $v_0 = 3$ m/s and (b) $v_0 = 5$ m/s.

more than one set of output ports can be defined to ensure that progressive buckling continues even after the first buckle zone. In the next example, a relatively longer tube is considered with two sets of output port definitions. In addition, the advantage of using the proposed method for designing tubes undergoing oblique impacts is also presented.

### *5.2. Progressive Buckling under Oblique Impact*

This example considers a relatively longer tube with two sets of output port definitions to examine the utility of the proposed method for designing tubes undergoing oblique impacts. As a baseline, a thin-walled square tube 480 mm long, 80 mm wide and with uniform thickness of 1.5 mm is impacted by a rigid plate. The tube is constrained at one end, and an imperfection is added in the form of an 8 mm long and 1 mm thick patch close to the lower end of the tube on one of its faces. The schematic of the tube and location of the imperfection are shown in Fig. 14(a). The rigid plate, which has a mass of 400 kg, is given an initial velocity of 5 m/s in the axial direction. Two different loading scenarios are considered: a) a pure axial impact; and b) an oblique impact with a loading angle of 10° as shown in Fig. 14(b). The simulation time for both cases is 0.03 seconds.

Like in the previous example, a mesh convergence study is performed

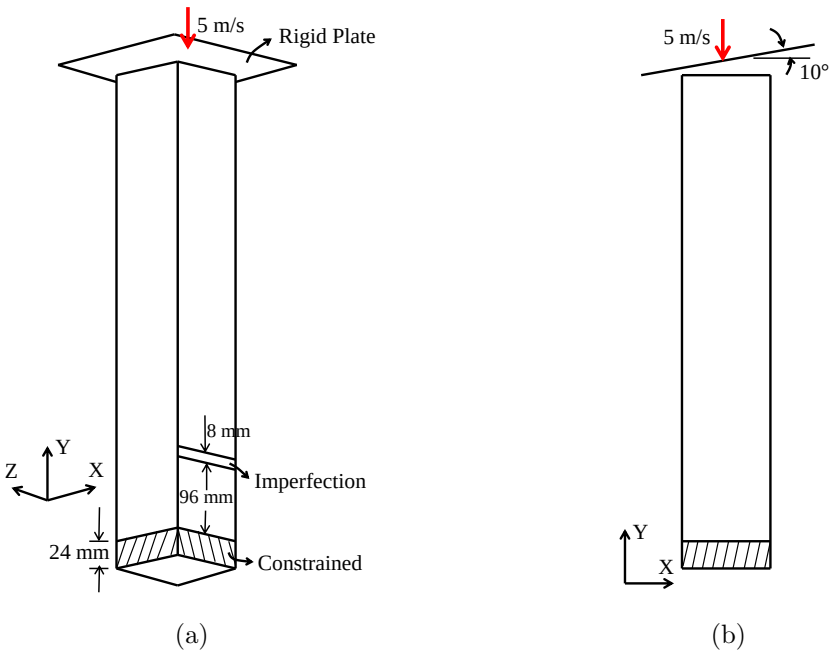


Figure 14: Schematic of a thin-walled square tube with an imperfection impacted by a rigid plate under (a) axial impact and (b) oblique impact at 10°.

with various mesh refinements for both the pure axial and oblique impacts. The results, corresponding to the four representative mesh sizes, are shown in Figs. 15 and 16. The force-time behavior of the model with the 80×60 mesh resolution for both axial and oblique impacts is significantly different than that of the other three models with finer mesh resolutions. During pure axial crushing, the first fold appears at the imperfection for all four models. The second fold forms above the first fold in the model with the 80×60 mesh resolution, whereas the second fold forms below the first fold in the other three finer mesh models. The peak force corresponding to the third fold in the model with the 80×60 mesh resolution is comparatively smaller than the corresponding force for the other three models. This results in less overall energy absorption in the 80×60 model during pure axial crushing, which can be seen in Fig. 16(a).

During the oblique impact, global bending in the 80×60 model starts a little later than in the other three models. This slight delay in the global bending results in comparatively lower energy absorption for the model with the 80×60 mesh resolution. The energy absorption values for the models with 160×240 and 240×240 mesh resolution are very close in the cases of both pure axial and oblique impacts. Hence, based on the force-time behavior, the amount of energy absorption, and the deformation pattern, a mesh resolution of 160×240 (element size of 2 mm × 2 mm) is found to be sufficient and used for the subsequent studies. Note that 160 is the number of elements along the square perimeter (40 elements on each face).

Figure 17 shows the deformation behavior of the uniformly thick tube with an imperfection under pure axial crushing by the rigid plate with an initial velocity of 5 m/s (Fig. 14(a)). The buckling starts at the imperfection and progresses in both directions afterwards. When the angle of impact is increased to 10° during the oblique loading, the tube undergoes Euler-type buckling (global bending) after a few folds form at the top as shown in Fig. 18. As found in similar studies [22, 23], the onset of global bending adversely affects the load carrying capacity and hence, the energy absorption. This can be confirmed by Fig. 19 in which the force-time and energy-time histories for the pure axial impact are compared with those for the oblique impact. The force drops to 0 and energy saturates once the tube loses contact with the rigid plate after the onset of global bending during the oblique impact.

In order to ensure that progressive buckling starts from the loading end during pure axial crushing and to avoid or delay the onset of global bending during the oblique impact, two sets of output ports close to the loading

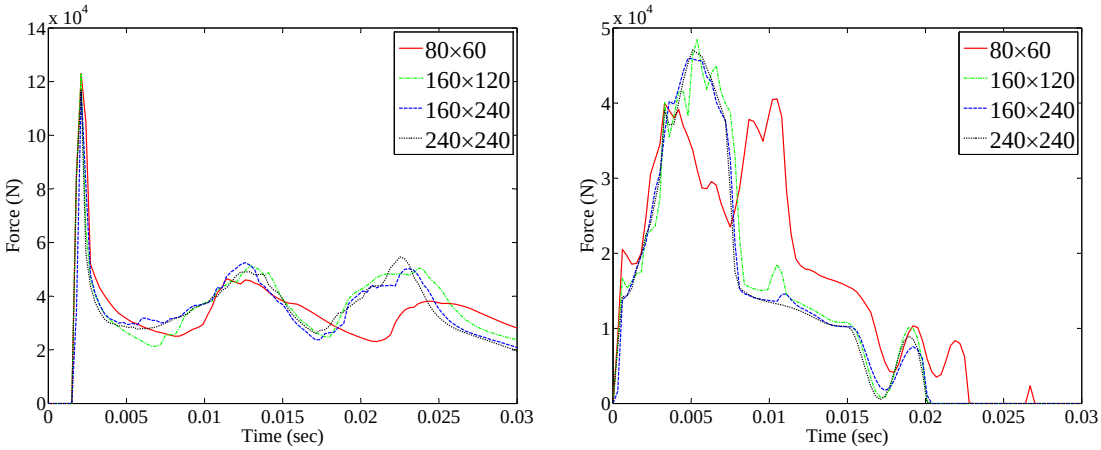


Figure 15: Mesh convergence study: Force-time behavior of the square tube modeled with four different mesh resolutions under (a) axial impact and (b) oblique impact at 10°.

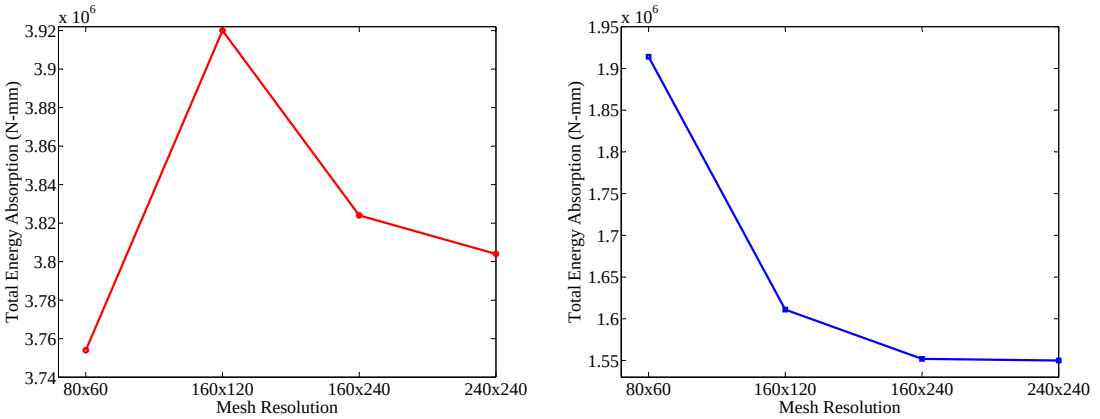


Figure 16: Mesh convergence study: Variation in the total energy absorption of a uniformly thick tube modeled with four different mesh resolutions for (a) axial impact and (b) oblique impact at 10°.

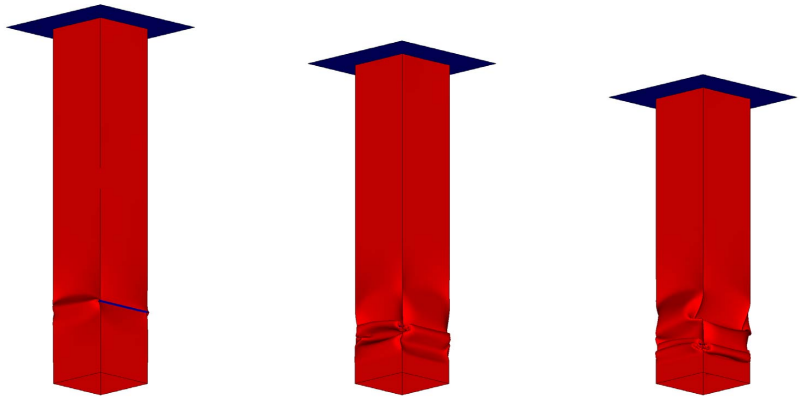

(a) (b) (c)

Figure 17: Deformation of the uniformly thick tube with an imperfection at various times when impacted axially by a rigid plate with an initial velocity of 5 m/s at simulation times (a) 0.0036 s, (b) 0.015 s, and (c) 0.030 s.

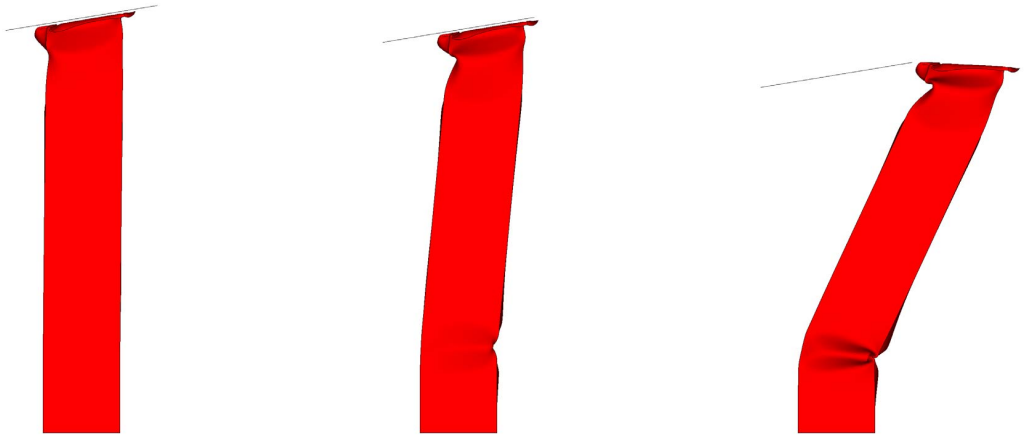

(a) (b) (c)

Figure 18: Deformation of the uniformly thick tube with an imperfection at various times when obliquely impacted at 10° by a rigid plate with an initial velocity of 5 m/s at simulation times (a) 0.006, (b) 0.009 s, and (c) 0.021 s. Note the onset of global bending in case (b).

end are defined in this example, as shown in Fig. 20(a). The second set is included in this case to maintain progressive buckling of the relatively longer tube length for a longer duration during the oblique impact so as to avoid or

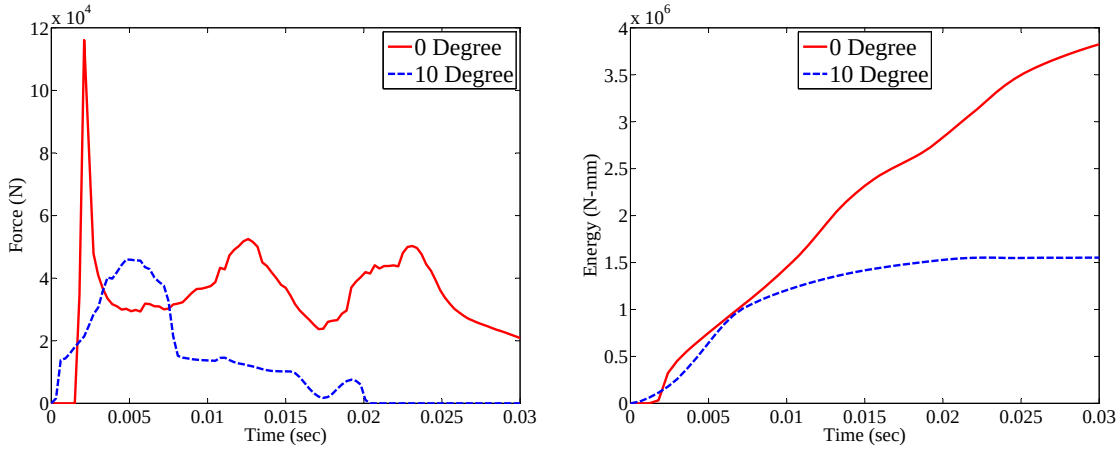


(a) (b)

Figure 19: Comparison of the dynamic response for the uniformly thick tube under axial and oblique impacts: (a) force vs. time and (b) energy vs. time.

delay the transition to global bending. The first set of output ports (pointing inward) are defined close to the loading end at a distance of 40 mm from the free end of the tube. The second set of output ports are defined 80 mm below the first set, assuming 40 mm to be half the wavelength of deformation in this case. A good starting point for deciding the relative distance between the output ports is to use the wavelength of deformation from the simulation of the original uniformly thick tube. However, a more rigorous technique would use the relative distance between the output ports as an additional design variable in a two-stage design method.

During the topometry design, the thickness variable in this case is allowed to vary between an upper bound ($t_{max}$) of 1.8 mm and a lower bound ($t_{min}$) of 1.2 mm. The average thickness target ($T^*$) is set to 1.5 mm so that the final mass of the designed tube remains the same as the mass of the original uniformly thick tube. As in the previous example, the imposed imperfection is not considered during the design process. Figure 20(b) shows the thickness distribution of the designed tube. As in the previous example, face A has an "hourglass" shape with a higher thickness (1.8 mm) in the first 80 mm of the tube length. This thickness distribution on face A, along with the thickness distribution on face B in the first 80 mm of the tube length, initiates a fold at a 40 mm distance from the free end corresponding to the location of the first set of output ports (O/P-1). In addition, a second smaller hourglass-shaped

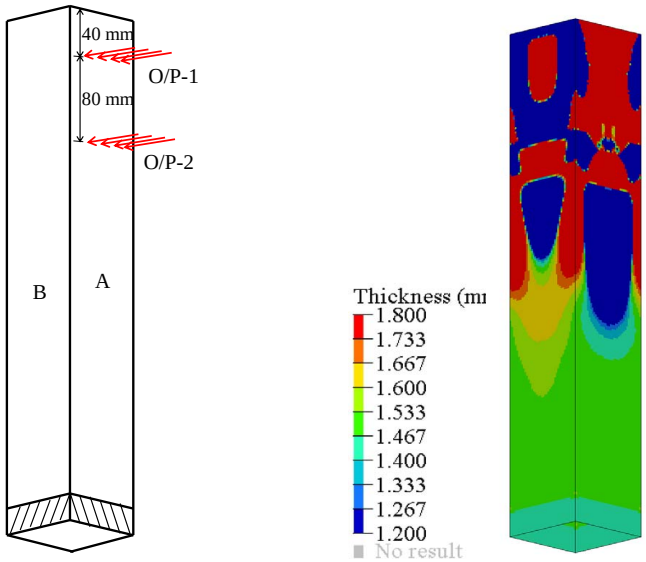


(a) (b)

Figure 20: Optimal design of a thin-walled structure with a single set of output ports: (a) output port definition and (b) thickness distribution for the designed tube.

thickness distribution on face A corresponds to the second set of output ports (O/P-2).

Figure 21 shows the deformation behavior of the designed tube under pure axial crushing. Note that the imperfection considered for the original uniformly thick tube is added back to the designed tube in order to make reasonable comparisons. As predicted, the buckling starts at the first set of output ports (Fig. 21(a)) in the prescribed symmetric mode, and it continues downwards. Moreover, the tube also buckles at the location corresponding to the second set of output ports (Fig. 21(c)) in a desired fashion. This shows that the proposed method can design tubes with multiple predefined buckle zones.

Next, the designed tube is tested under oblique impact (10°), and the deformation behavior at various times is shown in Fig. 22. Unlike the uniformly thick tube, the designed tube continues to buckle progressively, completely avoiding the transition to global bending. This behavior of the designed tube represents an increase in the load-carrying capacity compared to the uniformly thick tube, which can be seen in Fig. 23(a). Also, the increase in the load-carrying capacity means more energy absorption as shown in

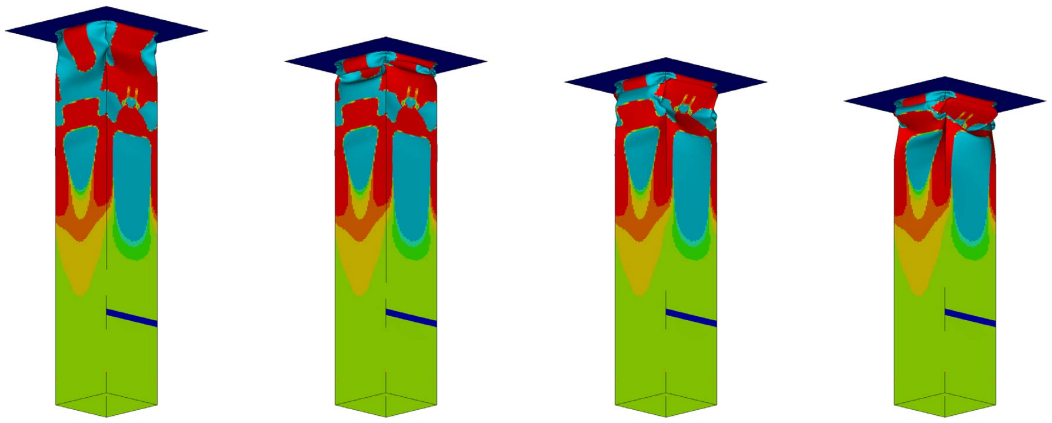

(a) (b) (c) (d)

Figure 21: Deformation of the designed tube with an imperfection at various times when impacted axially by a rigid plate with an initial velocity of 5 m/s for simulation times (a) 0.006 s, (b) 0.015 s, (c) 0.0222 s, (d) 0.030 s

Fig. 23(b). The designed tube absorbs $\sim$ 80% more energy than the uniformly thick tube during the simulation time of 0.03 seconds. Notably, the impact between the tube's lobes has a higher magnitude than the initial impact between the rigid wall and the free end of the tube. This situation is actually not uncommon during oblique impacts since the initial deformation of the tube's edge results in a reaction force of less magnitude than the one observed when the impact area increases below a folding lobe.

The present example has shown that the proposed method can be used to design long thin-walled square tubes with multiple predefined buckle zones. In addition, to enforce a progressive buckling starting from the loading end, these enforced buckle zones also can delay or avoid the onset of global bending during oblique impacts with load angles higher than the critical value. In both examples, a common trend in terms of design (hourglass shape) has been found that effectively triggers the buckling in a symmetric mode at desired locations along the length of the tube.

## 6. Discussion

The proposed design optimization method, based on compliant mechanism design and displacement maximization of output ports, enables the creation of enforced buckle zones that act as triggering mechanisms, even in

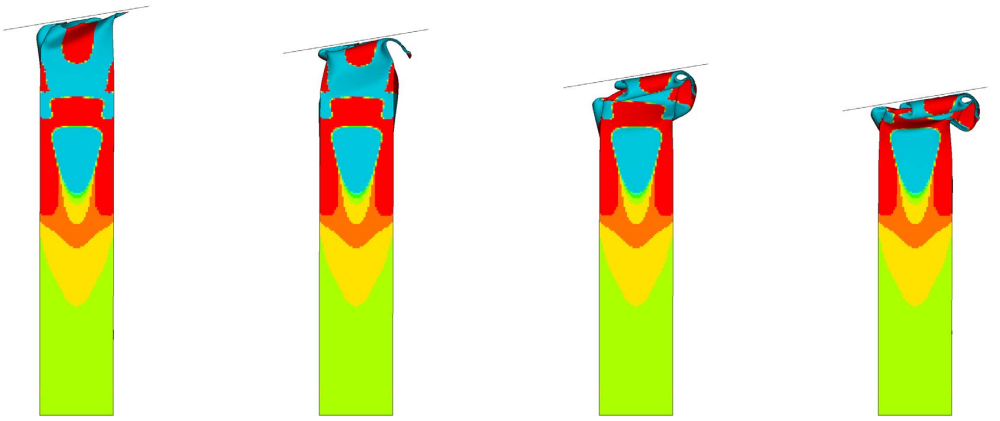

(a) t = 0.006 s (b) t = 0.012 s (c) t = 0.0222 s (d) t = 0.030 s

Figure 22: Deformation of the designed tube with an imperfection at various times when impacted obliquely (10°) by a rigid plate with an initial velocity of 5 m/s.

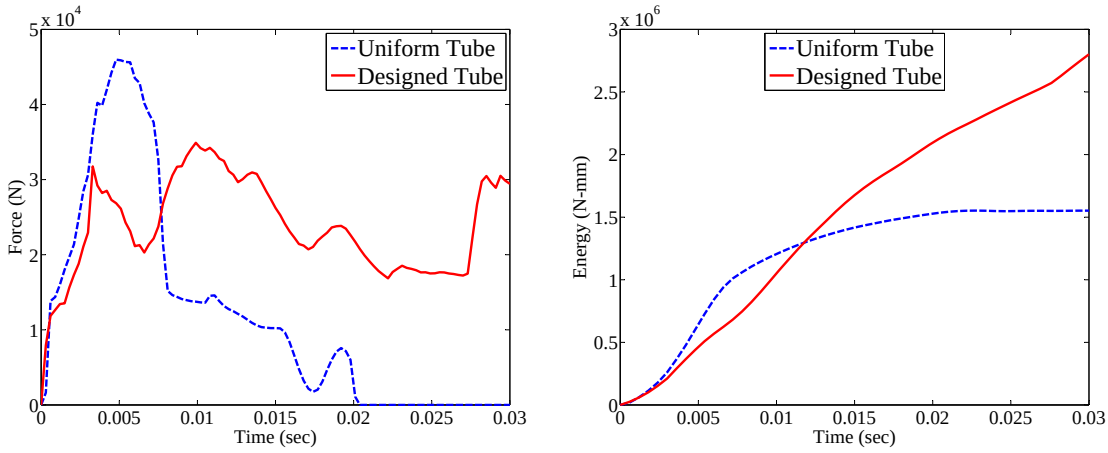


(a) Force-time history (b) Energy-time history

Figure 23: Comparison of the (a) force-time and (b) energy-time histories of the designed tube and the uniformly thick tube during the oblique impact.

the presence of geometric imperfections. This approach offers the benefits of: (a) initiating a specific axial collapse mode (symmetric in the present case), (b) stabilizing the collapse process, and (c) reducing the peak force, which is desirable for crashworthiness. The presence of enforced buckle zones in the top portion of the designed tubes helps to avoid or delay the onset of global

bending during oblique impacts with load angles higher than the critical value. Note that large imperfections and/or oblique loadings at a very high angle of impact may still result in undesirable behavior. Such cases should be handled differently, for example by improving the manufacturing process to reduce the imperfections and making changes in the basic geometry of the design to handle oblique loads with high impact angles. In addition to tubes with square cross sections, the present method can also be used for tubes with other regular cross sections such as rectangular, circular, polygonal, or even open sections like C and hat-shaped channels as long as the meshing is uniform.

The designed tubes with variable thickness distribution obtained with the present method are manufacturable with modern manufacturing techniques typically used for tailor-welded blanks (TWBs). A TWB is a part composed of different strengths or thicknesses of steel, joined usually by a laser weld. TWBs are increasingly gaining popularity among the automakers to reduce the weight of various sheet metal components without compromising the strength. Some common applications of TWBs in the automotive industry are the door inners, upper front rails, and B-pillars. Notably, if TWB is considered to fabricate the designed tubes, the effect of the welding must be included in the computational models.

The designs obtained with the present method can be simplified for ease of manufacture by grouping the elements based on their thicknesses. The elements with thickness near or equal to the upper bound ($t_{\max}$) are collected in one group and assigned a thickness of $t_{\max}$. Similarly, elements with a thickness close to the lower bound are collected in another group and assigned a thickness equal to $t_{min}$. All of the remaining elements whose thickness is generally close to the mean thickness ($T^*$) are placed in the last group, and a common thickness equal to $T^*$ is assigned to them. Figure 24 shows the result of using such a simplification by grouping the elements for the final design obtained in the first example. Since most of the elements in the final design have a thickness close to the upper bound, lower bound or mean value, the simplified design is very similar to the final design in terms of both thickness distribution and performance. These simplified designs with 3-4 discrete levels of thickness can be manufactured using patch tailor welded blanks. A patch TWB overlays one blank of material on top of another blank to add thickness (strength) where it is needed [36]. The two blanks are joined, usually by spot welds, before forming.

One of the limitations of the present method is the absence of a well-

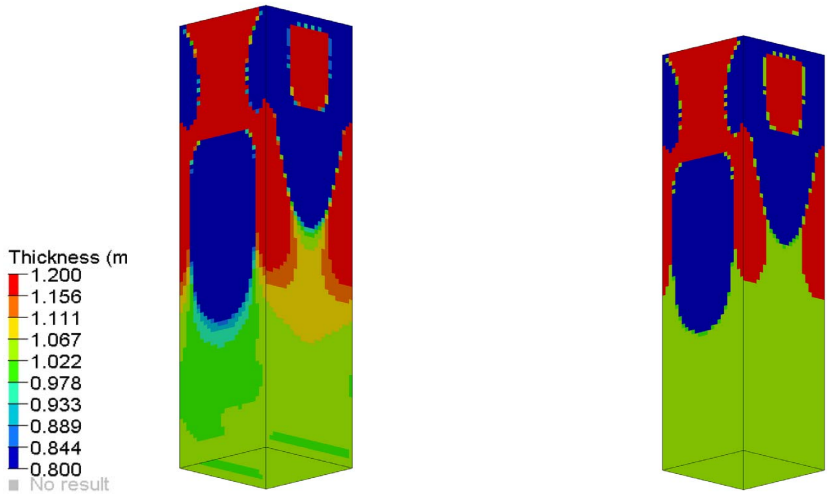


(a) Final design (b) Final design (after simplification)

Figure 24: (a) Final design from the first example and (b) simplified design after grouping the elements based on their thicknesses.

defined rule to decide the location of the first set of output ports and the distance between successive sets of output ports. Although it is reasonable to place these output ports based on the wavelength of deformation (distance between two successive folds) during the axial crushing of a uniformly thick tube, a more rigorous approach can be developed by incorporating the performance measures like peak force and energy absorption in deciding the port locations. For future work, the number of output ports and their locations along the length of the tube can be parameterized, and a two-stage design method can be formulated with the objectives of minimizing the peak force and maximizing the energy absorption.

## 7. Summary

This work introduces a new method for designing thin-walled tubes under axial and oblique impacts. The method consists of solving a compliant mechanism design problem within the thin wall of the structure. This design problem, posed as mutual potential energy maximization, relies on the definition of output ports. The location of the output ports, or enforced buckle zones, are in agreement with the wavelength of deformation during the axial crushing of a uniformly thick tube. In this work, the optimization problem

is solved using the HCA algorithm.

The optimization problem formulation includes mutual potential energy and mass functions. The results demonstrate improved crashworthiness in terms of a desirable progressive buckling and lower peak crushing force without increasing the structure's mass, with a less desirable reduction in total energy absorption. The results are demonstrated in thin-walled structures with width-to-thickness ratios $w/t > 40.8$, but there are no restriction to apply this approach to other configurations. Using the present method, square tubes can be designed to exhibit buckling starting from the loading (impact) end and systematically progressing toward the rear end, even in the presence of reasonable geometric imperfections and asymmetries in the loading conditions.

## 8. Acknowledgments

This material is based upon work supported by the Honda R&D Americas. Any opinions, findings and conclusions or recommendations expressed in this material are those of the author(s) and do not necessarily reflect the views of Honda R&D Americas.

[1] A. Pugsley, The Quarterly Journal of Mechanics and Applied Mathematics 13 (1960) 1–9.

[2] J. M. Alexander, The Quarterly Journal of Mechanics and Applied Mathematics 13 (1960) 10–15.

[3] W. Abramowicz, N. Jones, International Journal of Impact Engineering 2 (1984) 263–281.

[4] W. Abramowicz, International Journal of Impact Engineering 1 (1983) 309–317.

[5] T. Wierzbicki, W. Abramowicz, Journal of Applied Mechanics 50 (1983) 727–734.

[6] M. Langseth, O. S. Hopperstad, A. G. Hanssen, Thin-Walled Structures 32 (1998) 127–150.

[7] V. Tarigopula, M. Langseth, O. Hopperstad, A. Clausen, International Journal of Impact Engineering 32 (2006) 847–882.

[8] P. Fyllingen, O. Hopperstad, A. Hanssen, M. Langseth, Thin-Walled Structures 48 (2010) 134–142.

[9] Z. Kazanci, K.-J. Bathe, International Journal of Impact Engineering 42 (2012) 80 – 88.

[10] N. Jones, Structural Impact, Cambridge University Press, 1997.

[11] P. H. Thornton, C. L. Magee, Journal of Engineering Materials and Technology 99 (1977) 114–120.

[12] X. Zhang, G. Cheng, Z. You, H. Zhang, Thin-Walled Structures 45 (2007) 737–746.

[13] N. Chase, R. C. Averill, R. Sidhu, SAE world congress & exhibition (2009).

[14] H. El-Hage, P. K. Mallick, N. Zamani, International Journal of Crashworthiness 10 (2005) 183–196.

[15] S. Lee, C. Hahn, M. Rhee, J.-E. Oh, Materials & Design 20 (1999) 31–40.

[16] Y. Liu, Thin-Walled Structures 46 (2008) 1329–1337.

[17] A. Najafi, M. Rais-Rohani, Thin-Walled Structures 49 (2011) 1–12.

[18] X. Zhang, G. Cheng, International Journal of Impact Engineering 34 (2007) 1739–1752.

[19] F. Samer, F. Tarlochan, H. Samaka, International Journal of Research in Engineering and Technology 2 (2013) 109–116.

[20] S. Salehghaffari, M. Rais-Rohani, A. Najafi, Thin-Walled Structures 49 (2011) 397–408.

[21] S. C. K. Yuen, G. N. Nurick, Applied Mechanics Reviews 61 (2008) 020802.

[22] D. C. Han, S. H. Park, Thin-Walled Structures 35 (1999) 167–184.

[23] A. Reyes, M. Langseth, O. S. Hopperstad, International Journal of Mechanical Sciences 44 (2002) 1965–1984.

[24] C. Mozumder, J. E. Renaud, A. Tovar, Thin-Walled Structures 60 (2012) 100–120.

[25] P. Bandi, A. Tovar, J. E. Renaud, in: Proceedings of the 52nd AIAA Structures, Strucutural Dynamics, and Materials Conference, Denver, CO.

[26] O. Sigmund, Mech. Struct. & Machines 25 (1997) 495–526.

[27] M. P. Bendsøe, O. Sigmund, Topology Optimization: Theory, Methods and Applications, Springer-Verlag, Berlin, 2003.

[28] M. I. Frecker, G. K. Ananthasuresh, S. Nishiwaki, N. Kikuchi, S. Kota, Journal of Mechanical Design 119 (1997) 238–245.

[29] A. Saxena, , G. K. Ananthasuresh, Struct. Multidisc. Optim. 19 (2000) 36–49.

[30] A. Tovar, N. M. Patel, G. L. Niebur, M. Sen, J. E. Renaud, Journal of Mechanical Design 128 (2006) 1205–1216.

[31] A. Tovar, K. Khandelwal, Engineering Structures 48 (2013) 674 – 682.

[32] P. Bandi, J. P. Schmiedeler, A. Tovar, Journal of Mechanical Design 135 (2013) 091002.

[33] N. Peixinho, N. Jones, A. Pinho, Journal de Physique IV 110 (2003) 717–722.

[34] J. Hallquist, LS-DYNA theoretical manual, Livermore software technology corporation (LSTC), 2006.

[35] R. L. Weber, K. V. Manning, M. W. White, College Physics, McGraw-Hill, 4th edition, 1965.

[36] Tailor welded blank applications and manufacturing - A state-of-the-art survey, Technical Report, The Auto/Steel Partnership, 2001.